Running Title: Immunoglobulin M regulates airway hyperresponsiveness independent of T helper 2 allergic inflammation.

Authors and Affiliations:

Sabelo Hadebe[a*], Anca Flavia Savulescu[b], Jermaine Khumalo[a], Katelyn Jones[a], Sandisiwe Mangali[a,c], Nontobeko Mthembu[a], Fungai Musaigwa[a], Welcome Maepa[b], Hlumani Ndlovu[b], Amkele Ngomti[a,] Martyna Scibiorek[a,c], Javan Okendo[b,e], Frank Brombacher[a,c,d*]

[a]Division of Immunology, and South African Medical Research Council (SAMRC) Immunology of Infectious Diseases, Department of Pathology, Faculty of Health Sciences, University of Cape Town, Cape Town, South Africa

[b]Division of Chemical, Systems & Synthetic Biology, Faculty of Health Sciences, Institute of Infectious Disease & Molecular Medicine, University of Cape Town, Cape Town, South Africa

[c]International Centre for Genetic Engineering and Biotechnology (ICGEB) and Institute of Infectious Diseases and Molecular Medicine (IDM), Division of Immunology, Health Science Faculty, University of Cape Town, Cape Town, South Africa

[d]Wellcome Centre for Infectious Diseases Research in Africa (CIDRI-Africa), Institute of Infectious Diseases and Molecular Medicine (IDM), Faculty of Health Sciences, University of Cape Town, Cape Town, 7925, South Africa

[e]Centre for Research in Therapeutic Sciences (CREATES), Strathmore University, Nairobi, Kenya

26 * **Corresponding Author**: Professor Frank Brombacher

27 International Centre for Genetic Engineering and Biotechnology (ICGEB) and Institute

28 of

29 Infectious Diseases and Molecular Medicine (IDM), Division of Immunology, Health

30 Science

31 Faculty, University of Cape Town, Cape Town, South Africa

32 Email: brombacherfrank@gmail.com

33 Tel: +27 21 406 6424

34 Fax: +27 21 406 6938

35

36 * **Corresponding author:** Dr Sabelo Hadebe

37 Division of Immunology, Health Science Faculty, University of Cape Town, Cape

38 Town, South Africa

39 Email: sabelo.hadebe@uct.ac.za

40 Tel: +27 21 406 6161

41 Fax: + 27 21 406 6029

42

43

Abstract

Allergic asthma is a disease driven by T helper 2 (Th2) cells, eosinophilia, airway hyperresponsiveness (AHR) and IgE-secreting B cells. Asthma is largely controlled by corticosteroids and β_2 adregenic receptor agonists that target and relax airway smooth muscle (ASM). Immunoglobulin M (IgM) isotype secreted by naïve B cells is important for class switching but may have other undefined functions.

We investigated the role of IgM in a house dust mite (HDM)-induced Th2 allergic asthma model.

We sensitised wild-type (WT) and IgM-deficient ($IgM^{-/-}$) mice with HDM and measured AHR, and Th2 responses. We performed RNA sequencing on the whole lung of WT and $IgM^{-/-}$ mice sensitised to saline or HDM. We validated our AHR data on human ASM by deleting genes using CRISPR and measuring contraction by single-cell force cytometry.

We found IgM to be essential in AHR but not Th2 airway inflammation or eosinophilia. RNA sequencing of lung tissue suggested that IgM regulated AHR through modulating brain-specific angiogenesis inhibitor 1-associated protein 2-like protein 1 (*Baiap2l1*) and other genes. Deletion of *BAIAP2L1* led to a differential reduction in human ASM contraction when stimulated with TNF-α and Acetylcholine, but not IL-13.

These findings have implications for future treatment of asthma beyond current therapies.

Keywords: Immunoglobulin M, B cells, airway hyperresponsiveness, airway smooth muscle; TH2 cells; single cell force cytometry; fluorescently labelled elastomeric contractible surface; CRISPR-Cas9; *BAIAP2L1*

69 **INTRODUCTION**

70 Immunoglobulin M (IgM) is the first antibody isotype expressed during B cell
71 development and the first humoral antibody responder, conserved across all species
72 from zebrafish to humans [1]. IgM can be divided into natural and antigen-induced IgM
73 and can either be membrane-bound IgM-type B cell receptor (BCR) or secreted IgM
74 [2,3]. Natural IgM plays multiple roles in homeostasis including scavenging and
75 clearance of apoptotic cell debris in conjunction with phagocytic macrophages, B cell
76 survival through tonic signals, lymphoid tissue architecture and prevention of
77 autoimmune diseases [4–6]. At mucosal sites, both natural and antigen-induced IgM play
78 a role in shaping healthy microbiota and IgM repertoire is also shaped by microbiota
79 [7,8]. Secreted IgM antigen complexes can connect signals via unique and shared
80 receptors, suggestive of a more pleiotropic role in homeostasis and disease states [9–
81 11].

82 Natural IgM and secreted IgM are essential in many infectious and non-infectious
83 diseases including those induced by parasites, fungi, bacterial, viral and autoimmune
84 diseases [11]. In *Plasmodium falciparum*, anti-α-gal IgM and anti-MSP1 directed
85 antibodies are protective against primary and secondary infections [12,13]. Mice deficient
86 of secreted IgM are susceptible to pulmonary *Cryptococcus neoformans* and *P. carinii*
87 infection partly due to reduced activation of innate and adaptive responses [14,15]. At
88 mucosal surfaces, IgM promotes healthy gut bacteria that is beneficial for homeostasis
89 such as Firmicutes and Bacteroidetes [16]. Natural and induced secreted IgM produced
90 mainly by B1a cells is protective against *Streptococcus pneumoniae* and *Francisella*
91 *tularensis* infection [17,18]. In these settings, the protective effects of sIgM depended on

92 cytokines IL-1β and GM-CSF [17,18]. The involvement of natural or induced IgM in allergic
93 asthma is unknown, despite selective IgM syndrome dominated by asthma patients [19].
94
95 Asthma is a T helper 2 (Th2) disease characterised by eosinophilic lung inflammation,
96 mucus production, airway hyperresponsiveness (AHR), Th2 cytokines (interleukin-4
97 (IL-4), IL-5 and IL-13) and B cells producing IgE [20]. IgM is central to class switch
98 recombination that results in IgE class switched B cells [21]. We and others recently
99 showed that that the role of B cells in asthma is complex, where the load of the antigen
100 is crucial in their function [22–24]. Mice deficient of B cells ($\mu MT^{-/-}$) can mount exaggerated
101 AHR when challenged with house dust mite (HDM) [24–26] or ovalbumin (OVA) [27–29] partly
102 due to lack of regulatory B cells that dampen AHR [23]. Furthermore, interleukin 4
103 receptor alpha signalling in B cells is required for optimal Th2 allergic airway
104 inflammation through regulation of AHR, germinal centre (GC) formation and B
105 effector 2 function [22].
106
107 Interestingly, B cell isotypes show unique functions in allergic asthma, for example IgE
108 and its high affinity receptor, FcεR are redundant in an HDM model [30], whereas IgD
109 plays an amplifying and regulatory role in various allergic models [31]. In this context IgD
110 activate basophils to secrete IL-4 and Th2 induction during the sensitisation stage
111 through binding basophils via galectin-9 and CD44. Once Th2 responses have been
112 amplified, IgD ligation blocked IgE-mediated basophil degranulation through
113 competing for antigen and inhibiting FcεR mediated signalling [31]. How IgM isotype
114 contributes in the development of allergic asthma is unclear. It is also unclear whether
115 secreted IgM plays different roles compared to membrane bound IgM, which is more
116 likely to undergo class switching to IgE. We challenged mice lacking both membrane

and secreted IgM with HDM and other allergens and found a profound reduction in AHR. RNA sequencing of lung tissue showed a downregulation of brain-specific angiogenesis inhibitor 1-associated protein 2-like protein 1 (*Baiap2l1*) and erythroid differentiation regulatory factor 1 (*Erdr1*) genes associated with actin cytoskeleton and rearrangement smooth muscle contraction. As a proof of principle, we showed in human smooth muscle cell line that deletion of these genes via CRISPR- resulted in reduction in smooth muscle contraction at a single cell level. These are unexpected functions of secreted, and membrane bound IgM; namely, its involvement in modulating airway smooth muscle contraction.

128 **METHODS**

129 **Mice**

130 IgM-deficient homozygotes mice on Balb/C background and on C57BL/6 background
131 were backcrossed at least 10 generations [32]. Wild type on Balb/C and C57BL/6
132 backgrounds were used as a littermate control. Mice were housed in independently
133 ventilated cages under specific pathogen-free conditions at the University of Cape
134 Town Animal Facility. All mice were used at eight to 10 weeks of age and animal
135 procedures were performed according to the strict recommendation by the South
136 African Veterinary Council and were approved by the University of Cape Town Animal
137 Ethics Committee (Reference number 014/019, 018/013 and 022/014).

138

139 **House Dust-mite induced allergic airway disease**

140 A high dose and a low dose HDM treatment schedule were used to induce symptoms
141 of allergic asthma in mice [22]. Mice were anaesthetised with ketamine (Anaket-V;
142 Centaur Labs, Johannesburg, South Africa) and xylazine (Rompun; Bayer, Isando,
143 South Africa). For low-dose HDM, mice were sensitised intratracheally (i.t.) on day 0
144 with 1 µg of HDM (Stellergens Greer Laboratories, Lenoir, U.S.A.) and intranasally
145 challenged with 3 ug HDM on days 8, 9, 10, 11 and 12. For high-dose HDM, mice
146 were with HDM 100 ug and challenged with HDM 10 ug. AHR was measured on day
147 15. After the procedure, mice were euthanised and tissue samples were collected for
148 analysis.

149

150 **Adoptive transfer of naïve B cells**

151 Spleens were collected from naïve congenic CD45.1 Balb/C mice and passed through
152 40µm strainer to obtain single-cell suspensions. Cells were stained with FITC-B220

153 and APC-CD19 for 30min at 4°C. A dead cell exclusion dye (7AAD) was added before
154 sorting on BD FACS Aria I to at least 96% purity. 2-5 x 10^6 cells were adoptively
155 transferred intravenously (i.v.) into $IgM^{-/-}$ recipient mice a day before HDM
156 sensitisation.
157
158 **Adoptive transfer of naïve serum**
159 Naïve wild-type mice were euthanised and blood was collected via cardiac puncture
160 before being spun down (5500rpm, 10min, RT) to collect serum. Serum (200μL) was
161 injected intraperitoneally into IgM-deficient mice, 1 day before sensitisation with HDM.
162 In some experiments, serum was injected intraperitoneally at day -1, 0, and a day
163 before challenges.
164
165 **Ovalbumin-induced allergic airway inflammation**
166 Mice were sensitised intraperitoneally with (50μg in 200μl) of ovalbumin (OVA)
167 adsorbed to 0.65% alum (Sigma-Aldrich, Aston Manor, South Africa) on days 0, 7, 14.
168 On days 23, 24, 25, mice were intranasally challenged with 100μg of OVA under
169 anaesthesia with ketamine (Anaket-V; Centaur Labs, Johannesburg, South Africa)
170 and xylazine (Rompun; Bayer, Isando, South Africa). AHR was measured on day 26.
171 After the procedure, mice were euthanized with halothane and tissue samples
172 collected for analysis.
173
174 **Papain-induced lung inflammation**
175 Mice were anaesthetized with isoflourane (3L/min) briefly before being challenged with
176 50μL of 25 μg of Papain (Sigma-Aldrich, Aston Manor, South Africa) on days 1, 2 and

177 3 or PBS. AHR was measured on day 4. After the procedure, mice were euthanized
178 with halothane and tissue samples collected for analysis.
179
180 **Airway Hyperresponsiveness**
181 Airway resistance and elastance of the whole respiratory system (airways, lung chest
182 wall) after intranasal challenge was determined by forced oscillation measurements
183 as described previously [33] with the Flexivent system (SCIREQ, Montreal, Canada) by
184 using the single compartment (''snapshot'') perturbation. Measurements were carried
185 out with increasing doses of acetyl-β-methylcholine (methacholine, Sigma-Aldrich,
186 Aston Manor, South Africa) (0, 5, 10, 20 and 40 mg/mL) for Balb/C or (0, 20, 40, 80
187 160 and 320 mg/mL) for C57BL/6. Differences in the dose-response curves were
188 analysed by repeated-measures Two-way ANOVA with the Bonferroni post-test. Only
189 mice with acceptable measurements for all doses (coefficient of determination >0.90)
190 were included in the analysis.
191
192 **Flow cytometry**
193 Single-cell suspensions were prepared from lymph nodes in Roswell Park Memorial
194 Institute (RPMI) media (Gibco, Paisley, United Kingdom) by passing them through
195 100µm strainer. To obtain single cell suspensions from lung tissues, a left lobe was
196 digested for 1 hour at 37°C in RPMI containing 13 mg/mL DNase I (Roche, Randburg,
197 South Africa) and 50 U/mL collagenase IV (Gibco, Waltham, Massachusetts) and
198 passed through 70µm strainer. Antibodies used in these experiments included,
199 phycoerythrobilin (PE)- conjugated anti-Siglec-F (clone, E50-2440), anti-IL-5 (clone,
200 TRFK5), anti-CD44 (clone, KM114), anti- T and B cell activation antigen (clone, GL7),
201 anti-CD43 (clone, S7), FITC- conjugated anti-Ly6G (clone, 1A8), anti-IgD (clone, 11-

202 26C2a), IL-4 (clone, 11B11), anti-PD-1-(clone, 29F.1A12), PerCP Cy5.5- conjugated
203 anti-Ly6C (clone, AL-21), -CD45.1 (clone, A20), anti-IL-17 (clone, TC11-18H10), anti-
204 mouse alpha muscle actin (Abcam, ab8211-500), Allophycocyanin (APC)- conjugated
205 anti-CD11c (clone, HL3), anti-CD5 (clone, 53-7.3), BV421 conjugated anti-CD11b
206 (clone, M1/70), anti-CD62L (clone, MEL-14), anti-IgG1 (clone, A110-1), AlexaFlour
207 700- conjugated anti-CD3ε (clone, 145-2C11) -anti-IFN-γ (clone, XMG1.2), BV510-
208 anti-CD4 (clone, RM4-5) and anti- B220 (clone, RA3-6B2), APC-Cy7-conjugated anti-
209 CD19 (clone, 1D3) and anti-CD8 (clone, 53-6.7), BV786 conjugated anti-IgE (clone,
210 R35-72) and anti-IL-33R (ST2) (clone, U29-93), biotin-conjugated anti-IgM (clone, AF-
211 78), anti-CD95 (clone, Jo2), anti- CD249 (clone, BP-1) , anti-CD45 (clone, 30-F11)
212 were purchased from BD Pharmingen (San Diego, CA). PE-Cynanine7 anti-F4/80
213 (clone, BM8), anti-IL-13 (clone, eBio13A), anti-CXCR5 (clone, L138D7), AlexaFlouro
214 700- conjugated anti-MHC II (clone, M5/114), Rabbit anti-BAIAP2L1 (Abcam,
215 PA554000), Live/dead Fixable Yellow stain (Qdot605 dead cell exclusion dye) were
216 purchased from eBiosciences. Biotin-labelled antibodies were detected by Texas Red
217 conjugated PE (BD Biosciences). PE-Goat anti-Rabbit IgG (Abcam, ab72465) was
218 used to detect Rabbit anti-BAIAP2L1. For staining, cells (1 x 10^6) were stained and
219 washed in PBS, 3% FCS FACS buffer. For intracellular cytokine staining, cells were
220 restimulated with phorbal myristate acetate (Sigma-Aldrich) (50 ng/mL), ionomycin
221 (Sigma-Aldrich) (250ng/mL), and monensin (Sigma-Aldrich) (200mM in IMDM/10%
222 FCS) for 5h at 37˚C then fixed in 2% PFA, permeabilised with Foxp3 transcriptional
223 factor staining buffer kit (eBioscience) before intracellular staining with appropriate
224 cytokine antibodies and acquisition through LSR Fortessa machine (BD
225 Immunocytometry system, San Jose, CA, USA) and data was analysed using Flowjo
226 software (Treestar, Ashland, OR, USA).

227 **Histology**

228 Left upper lung lobes was fixed in 4% formaldehyde/PBS and embedded in paraffin.
229 Tissue sections were stained with periodic acid-Schiff for mucus secretion, and
230 haematoxylin and eosin (H&E) stain for inflammation. Slides were scanned at 20x
231 magnification on the virtual slide VS120 microscope (Olympus, Japan). Downstream
232 processing of images was done through Image J (FIJI) for image extraction at series
233 15 and Ilastik software was used for mucus area quantification on whole lung sections.
234 The data shown are representative of 1 experiment of 3 independent experiments (n
235 = 5-7 mice per experiment).

236

237 **Antibody and cytokine ELISAs**

238 Antibody ELISAs were carried out as previously described[33] using 10 μg/ml HDM to
239 coat for specific IgGs. Total IgE in serum was measured using anti-mouse IgE (BD
240 Biosciences, 553413) to coat, mouse IgE (κ, anti-TNP, BD Biosciences, 557079) as
241 standard and biotin anti-mouse IgE (BD Biosciences, 553419) as a secondary
242 antibody.

243 For *in vitro* cytokine production analysis, single-cell suspensions were prepared from
244 mediastinal lymph nodes of HDM-treated and littermate control mice. Cells ($2x10^5$
245 cells, in 200μL) were incubated for 5 days in RPMI/10% FCS (Delta Bioproducts,
246 Kempton Park, South Africa) in 96-well plates. Cells were either stimulated with HDM
247 (30μg/mL) or plate bound anti-CD3 (10μg/mL) and supernatants were collected after
248 a 5-day incubation period. Concentrations of IL-4, IL-5 (BD Biosciences) and IL-13
249 (R&D Systems, Minneapolis, Minn), were measured using ELISA assays according to
250 the manufacturer's protocol.

251

252 **RNA Extraction**

253 Small lung lobe was frozen in Qiazol (Qiagen, Germany) and stored at −80°C. Total
254 RNA was isolated from the lysate using miRNeasy Mini kit (Qiagen, Germany)
255 according to the manufacturer's instructions. RNA quantity and purity were measured
256 using the ND-1000 NanoDrop spectrophotometer (ThermoScientific, DE, USA).

257

258 **cDNA Synthesis and RT-qPCR**

259 For *Muc5a* gene expression analysis, 100 ng total RNA was reverse transcribed into
260 cDNA using Transcriptor First Strand cDNA Synthesis Kit (Roche, Germany)
261 according to the manufacturer's instructions. Quantitative real-time PCR (RT-qPCR)
262 was performed using LightCycler® 480 SYBR Green I Master (Roche, Germany) and
263 *Muc5a* primers (IDT, CA, USA). Fold change in gene expression was calculated by
264 the ΔΔCt method and normalized to ß-*actin* which was used as an internal control.

265

266 **Whole lung RNA sequencing**

267 Whole lung RNA was extracted using RNAeasy kit (Qiagen, Germany) according to
268 the manufacturer's instructions. We used Agilent 2100 Bio analyzer (Agilent RNA 6000
269 Nano Kit) to do the total RNA sample QC: RNA concentration, RIN value,28S/18S and
270 the fragment length distribution. The first step in the workflow involved purifying the
271 poly-A containing mRNA molecules using poly-T oligo attached magnetic beads.
272 Following purification, the mRNA was fragmented into small pieces using divalent
273 cations under elevated temperature. The cleaved RNA fragments were copied into
274 first strand cDNA using reverse transcriptase and random primers. This was followed
275 by second strand cDNA synthesis using DNA Polymerase I and RNase H. These
276 cDNA fragments had addition of a single 'A' base and subsequent ligation of the

277 adapter. The products were then purified and enriched with PCR amplification. PCR
278 yields were quantified by Qubit and pooled samples together to make a single strand
279 DNA circle (ssDNA circle), which gave the final library. DNA nanoballs (DNBs) were
280 generated with the ssDNA circle by rolling circle replication (RCR) to enlarge the
281 fluorescent signals at the sequencing process. The DNBs were loaded into the
282 patterned nanoarrays and pair-end reads of 100 bp were read through on the DNBseq
283 platform for the following data analysis study. For this step, the DNBseq platform
284 combines the DNA nanoball-based nanoarrays and stepwise sequencing using
285 Combinational Probe-Anchor Synthesis Sequencing Method.
286
287 **Bioinformatics workflow**
288 The ribosomal RNA (rRNA) was first removed using SortMeRNA. We then did the
289 Fastq file quality control using Fastqc and multiqc software to assess the quality of the
290 raw reads followed by adapter trimming using Trim galore. The reads were then
291 aligned to the mouse reference genome (mm10_UCSC_20180903) using STAR
292 aligner. The map read counts was then extracted using featurecounts. The gene
293 differential analysis was conducted using the DEseq2. The genes with LFC >= 2 and
294 adjusted p-value <= 0.05 was used to do the gene ontology over-representation
295 analysis done using clusterProfiler[34] Bioconductor package. The Benjamini-Hochberg
296 method was used for multiple test correction.
297
298 **Human bronchial Airway Smooth Muscle cell culture**
299 A healthy human bronchial smooth muscle cell line (BSMC, Lonza) was cultured in
300 Smooth Muscle Growth Medium (Lonza) supplemented with Insulin (CC-4021D),
301 human Fibroblastic Growth Factor-B (CC-4068D), Gentamicin sulfate-Amphotericin-

302 1000 (CC-4081D), 5% Foetal Bovine Serum (CC-4102D), human Epidermal Growth
303 Factor (CC-4230D) (all purchased from Lonza) in a T25 flask (Lonza) until confluence.
304 After two passages in the T75 flask, confluent cells were seeded at 1.6×10^5 BSMC
305 cells onto 24-well trays and immediately transfected with CRISPR/Cas9 single guide
306 RNAs.
307
308 **CRISPR/Cas9 single guide RNA transfections**
309 single guide RNAs targeting human *BAIAP2L1* (# CD.Cas9.CXVQ6494.AA); *ERDR1*,
310 (# CD.Cas9.YFVV2490.AA); HPRT Negative Control (#Alt-R® CRISPR-Cas9crRNA)
311 were purchased (IDT, CA, USA via WhiteScientific PTY LTD). Single guide RNA (1
312 μM) and Cas9 enzyme (1 μM) in Opti-MEM medium (Life Technologies™, Carlsbad,
313 CA, USA) were transfected using Lipofectamine RNAi Max 1000 (Thermo Scientific)
314 into BSMC cells (1.6×10^5) per well and either stimulated with Acetylcholine (10μM),
315 recombinant human IL-13 (100 ng/mL), recombinant human TNF-α (10 ng/mL) or left
316 unstimulated for 48 hours at 37°C, 5% CO_2 incubator. Gene deletion was confirmed
317 by DNA extraction (Wizard Genomic DNA Purif. Kit, Promega) and PCR amplification
318 of target genes using *BAIAP2L1* forward (GTCCCGGGGGCCCGA) and reverse
319 (AAGCGCCCAAGAATGTGGGG) primers, and product run on a 1.2% agarose gel.
320
321 **Cytotoxic detection Assay**
322 To measure cytotoxicity after single guide RNA transfection, lactate dehydrogenase
323 (LDH) was measured in supernatants collected at 48 hours post transfection using
324 cytotoxicity detection kit ^{PLUS} Assay (CYTODET-RO, Roche) according to
325 manufacturer's instructions and plates were read at 490 nm.
326

327 **Single-cell force cytometry using Fluorescently Labelled Elastomeric**
328 **Contractible Surface (FLECS) technology**

329 BSMCs were seeded on Fibronectin-coated elastomeric micropatterns (Forcyte
330 Biotechnologies #F2AX0G03Y, 50 microns, Alexa Fluor 488 - bound Fibrinogen, 24-
331 well plate) at a concentration of 75,000 cells per well in Smooth muscle growth medium
332 (SmGM) (Lonza) and left to adhere and spread for 90 minutes. Unattached cells were
333 then removed and fresh SmGM medium supplemented with rhTNF-α (10 ng/mL)/rhIL-
334 13 (100 ng/mL)/ACh (10μM) was added. BSMCs were stimulated for 3 hrs before
335 being fixed in pre-warmed to 37°C 4% PFA. Fixed samples were washed and then
336 stained with ATTO-565 phalloidin (ATTO-TEC) and DAPI (Life Technologies) and
337 imaged on a StellarVision microscope using Synthetic Aperture Optics technology
338 (Optical Biosystems). All images were analyzed using FiJi software by measuring the
339 length of each micropattern per condition after stimulation and subtracting the length
340 of the unstimulated micropattern of the same condition.

341

342 **Immunofluorescent**

343 Left upper lung lobes were fixed in 4% formaldehyde/PBS and embedded in paraffin.
344 Tissue sections (5 μm) were deparaffinised and hydrated in water before antigen
345 retrieval in boiling 10 mM Citrate buffer (pH 6, pressure cooker for 2 mins). Tissue was
346 incubated with Rabbit anti-BAIAP2L1 (Abcam, PA554000) in PBS-Tween (1:250,
347 overnight, 4°C) and FITC anti-mouse alpha muscle actin (Abcam, ab8211-500, 1:100,
348 overnight, 4°C). Tissues were washed with PBS-Tween before incubation with
349 secondary antibody PE-Goat anti-Rabbit IgG (Abcam, ab72465) in PBS-Tween
350 (1:500, RT in the dark for 30min). Tissues were washed with PBS-Tween before

351 mounting in DAPI mounting media (Thermofisher). Fluorescent images were captured
352 at 60x magnification using LSM880 Airy Scan (Zeiss, UK).
353
354 **Western blotting**
355 Protein harvest: RIPA lysis buffer supplemented with protease inhibitors was added to
356 the lung tissue. The whole-cell lysates were incubated on ice for 20 min and vortexed
357 every 5 min for 60 seconds. Then, the lysate was centrifuged at 3000 rpm for 15
358 minutes at 4°C, and the supernatant was collected. Total protein concentrations were
359 determined using the Pierce BCA Assay kit.
360
361 SDS-PAGE: 20 µg of each protein sample was mixed with Laemmli buffer and heated
362 for 10 minutes at 100 °C. Equal amounts of protein samples were loaded into 5%
363 acrylamide stacking gel and a 12% acrylamide separating gel along with 5 µL
364 PageRulerTM Plus Prestained protein ladder (catalogue #: 26619, Thermo
365 ScientificTM) and separated by electrophoresis at 100 V. Proteins were transferred
366 onto nitrocellulose membranes (Bio-Rad) using the Bio-Rad Mini Trans-Blot® Cell
367 according to the manufacturer's instructions.
368
369 After protein transfer, the nitrocellulose membranes were stained with Ponceau stain
370 for approximately 1-3 minutes to visualize if the proteins had been transferred. Once
371 the protein bands were identified, the membrane was washed with ddH_2O until 80%
372 of the Ponceau staining is removed. The remaining 20% of the stain allowed the
373 accurate segmentation of the membrane to separate high molecular weight proteins
374 from low molecular weight proteins. The nitrocellulose membranes were blocked with
375 5 % (w/v) non-fat milk, 0.01% Tween-20 in TBST) on the shaker at room temperature

376 for one hour. The low and high molecular weight membranes proteins were incubated
377 with respective primary antibodies (Rabbit anti-human BAIAP2L1, PA5-54000,
378 Invitrogen) or (Goat anti-mouse GAPDH, sc 365062, Santa Cruz) overnight shaking
379 in the 4°C cold room. Membranes were washed 4 times with 1xTBST in 15-minute
380 intervals. Horseradish peroxidase (HRP) secondary antibodies were added to their
381 respective membranes and incubated for one hour at room temperature, with shaking.
382 subsequently, membranes were washed 3 times in 1xTBST in 15 minutes intervals.
383 To visualise the protein bands on autoradiographic film (Santa Cruz Biotechnology®),
384 Lumino Glo® substrate kit was added to each membrane. Briefly, the substrate luminol
385 was oxidised by hydrogen peroxide in the presence of the catalyst HRP to yield a
386 chemiluminescent product.
387
388 **Plating of faecal pellets to confirm a reduction in bacterial colonies following**
389 **antibiotic treatment.**
390 The faecal pellet was collected from each individual mouse treated with antibiotics as
391 well as control groups not treated with antibiotics. The faecal pellet was weighed and
392 resuspended in sterile PBS at a concentration of 50 mg/mL. The sample was
393 resuspended until homogenous, and 1/100 dilution was made in sterile PBS. 50μL of
394 1/100 dilutions was plated on tryptic soy agar plates and spread evenly across the
395 plate before incubating at 37°C for 16 hrs. Individual colonies were counted manually.
396
397 **Statistical analysis**
398 P-values were calculated in GraphPad Prism 6 (GraphPad Software, Inc) by using
399 nonparametric Mann-Whitney Student's t-test or Two-way ANOVA with Bonferroni's
400 post-test for multiple comparisons, and results are presented as standard error of the

401 mean (SEM) or mean of standard deviation (SD). Differences were considered
402 significant if P was <0.05.
403
404

405 **RESULTS**

406 **IgM-deficient mice show profound airway hyperresponsiveness reduction when**
407 **exposed to HDM.**

408 We sensitised and challenged IgM-deficient (IgM$^{-/-}$) and wild-type Balb/c (WT) mice
409 with HDM intratracheally (i.t.) and analysed AHR, lung infiltrates and cytokines (Fig.
410 1a, Supplementary Fig. 1a). We found moderately reduced resistance and elastance
411 in IgM$^{-/-}$ sensitised with a high dose of HDM (100μg) compared to WT mice
412 (Supplementary Fig. 1b). Similarly, we also observed a profound reduction in AHR in
413 IgM$^{-/-}$ mice sensitised with a low dose of HDM (1μg) compared to WT (Fig. 1b).
414 Interestingly, lung eosinophils were intact at both low dose (Fig. 1c) and high dose
415 HDM (Supplementary Fig. 1d). We could also show that AHR reduction in IgM$^{-/-}$ mice
416 was not allergen-specific, as we observed similar findings using ovalbumin (OVA)
417 complexed to alum adjuvant (Supplementary Fig. 2a-b) and acute papain-induced
418 allergic inflammation (Supplementary Fig. 2c-d). We observed similar finding of
419 profound AHR reduction in IgM$^{-/-}$ mice in C57BL/6 background compared to WT mice
420 (Supplementary Fig. 3a). These findings suggested that IgM-deficient mice have
421 profound AHR reduction independent of allergen or mice background strain.

422

423 **IgM-deficiency does not impact B cell subsets in primary and secondary organs,**
424 **but class switching is impaired.**

425 We also observed no significant changes between IgM$^{-/-}$ and WT mice in mucus
426 production shown by *Muc5a* gene expression (Fig. 1d) or goblet cells in Balb/C
427 (Supplementary Fig. 1f) and C57BL/6 mice challenged with HDM (Supplementary Fig.
428 3b). Accompanying reduction in AHR in IgM$^{-/-}$ mice was low titers of total IgE, HDM-
429 specific IgE, and mediastinal lymph node (mLN) B cell surface expression of IgM and

430 IgG1 (Fig. 1e-f), owing to a lack of class switching. Interestingly, the numbers of lung
431 B cells were normal (Fig. 1c and Supplementary Fig. 1c) and the frequencies of B cell
432 subsets such as follicular, marginal zones and germinal centres (GCs) B cells were
433 not affected by lack of IgM (Fig. 1g and Supplementary Fig. 1g). The lack in class
434 switching in Balb/C mice was also consistent with what we found in $IgM^{-/-}$ mice in the
435 C57BL/6 background (Supplementary Fig. 3c). This suggested a normal interaction
436 between B and T cells in GCs, but lack of AID-dependent class switching, despite
437 increased expression of IgD (Supplementary Fig. 4a) [35]. We checked for natural IgM
438 and antigen-induced IgM in multiple tissues. B cells expressing IgD were increased in
439 all tissues including mLNs, peritoneal cavity and spleen (Supplementary Fig. 4a-c) and
440 pre-B cell subsets were normal in BM (Supplementary Fig. 4d) in the absence of IgM
441 as previously reported [32].
442

443 **T helper 2 cells are intact in the absence of IgM, and serum transfer can partially**
444 **restore antibody function**

445 To investigate whether the reduction in AHR was due to reduced Th2 cells and
446 cytokines, we stimulated total mLN and lung cells with anti-CD3 for 5 days or with
447 PMA/ionomycin for 5 hrs in the presence of monensin and measured secreted or
448 intracellular IL-4 and IL-13 expression. We found no differences in CD4 T cells and T
449 follicular helper cells (Fig. 2a) in mLN and in secreted or intracellular levels of IL-4 and
450 IL-13 between $IgM^{-/-}$ and WT mice challenged with HDM in both mLN and lungs (Fig.
451 2b-c). To investigate what drives this reduced AHR in the absence of IgM between
452 secreted antibodies or the IgM B cell receptor on the surface of B cells, we transferred
453 serum from naïve WT mice into $IgM^{-/-}$ mice a day before sensitization, during
454 sensitisation and a day before challenge with HDM allergen (Fig. 2d), as previously

455 described [36]. AHR in IgM$^{-/-}$ was still reduced compared to WT mice even after the
456 transfer of WT serum (Fig. 2e), but levels of total IgE, HDM-specific IgE and HDM-
457 specific IgG1 were increased and comparable to those found in WT mice (Fig. 2f and
458 Supplementary Fig. 5e). The redundant role of IgE was consistent with previous
459 studies where IgE nor its high-affinity receptor (FcεRI) were essential in AHR in an
460 HDM or OVA models [30]. The lack of functional role of serum-transferred IgE was
461 consistent with earlier findings on *H. polygyrus* transfer of immune serum where IgE
462 was found not to be essential in protection against *H. polygyrus* re-infection [36]. We
463 also tried to restore IgM function through adoptive reconstitution with congenic CD45.1
464 BM or sorted B cells into IgM$^{-/-}$ mice (Supplementary Fig. 5a). This approach did not
465 replenish IgM B cells to levels observed in WT mice and as a result did not restore
466 AHR, total IgE and IgM in these mice (Supplementary Fig. 5b-c). To understand why
467 we could not reconstitute IgM, we checked for transferred congenic B cells in different
468 organs after reconstitution with WT BM in IgM$^{-/-}$ mice and found some engraftment in
469 BM and spleen, but poor engraftment to lung and mLNs which may partially explain
470 our inability to restore AHR in IgM$^{-/-}$ mice challenged with HDM (Supplementary Fig.
471 5d).
472
473 IgM is known to play key role in shaping gut microbiota and its diversity can be shaped
474 by gut commensals [16,37]. To understand whether microbiota could influence AHR in
475 IgM-deficient mice, we treated WT and IgM$^{-/-}$ with an antibiotic cocktail 3x per week for
476 2 weeks (Supplementary Fig. 6a). We confirmed the reduction of bacteria in the faecal
477 pellet after 2 weeks of antibiotic treatment (Supplementary Fig. 6a). We then
478 sensitised and challenged these mice with HDM and measure AHR (Supplementary
479 Fig. 6b). We observed increased resistance and elastance in WT mice compared to

480 IgM$^{-/-}$ mice and pre-treatment with antibiotics did not influence AHR (Supplementary
481 Fig. 6b). Treatment with antibiotics did increase total IgE, HDM-specific IgE and IgG1
482 in WT mice as expected[38], but had no impact on IgM-deficient mice (Supplementary
483 Fig. 6c), suggesting that overall antibiotics did not influence AHR.
484
485 **RNA sequencing reveals enrichment of genes associated with skeletal muscle**
486 **contraction and actin re-arrangement.**
487 Because we had found no other changes in asthmatic allergic features between WT
488 and IgM$^{-/-}$, except for profoundly reduced AHR, we resorted to RNA sequencing to see
489 if there were lung-specific factors that influenced AHR regulation in IgM-deficient mice.
490 Principal component analysis (PCA) depicted distinct global transcriptional changes
491 with PC1 and PC2 explaining most of the variation (Fig. 3a). We found a smaller
492 variation in gene expression between WT and IgM$^{-/-}$ in both HDM-challenged and PBS
493 control mice (Fig. 3b). We could mainly detect downregulation of genes such as brain-
494 specific angiogenesis inhibitor 1-associated protein 2-like protein 1 (*Baiap2l1*),
495 erythroid differentiation regulatory factor 1 (*Erdr1*), chemokines such as *Ccl8*, *Ccl9*,
496 *Ccl17* and *Ccl22* in IgM$^{-/-}$ mice challenged with HDM (Fig. 3c-d). Interestingly, *Baiap2l1*
497 and *Erdr1* were also downregulated in IgM$^{-/-}$ saline-treated control mice, suggesting
498 an inflammation-independent effect (Fig. 3c and e). We also found the presence of the
499 J-chain coding gene in WT mice which was absent in IgM$^{-/-}$ mice, confirming a deletion
500 in genes associated with holding IgM monomers together and thus IgM [39] (Fig. 3e).
501 Gene set enrichment analyses (GSEA) confirmed that the genes contributing to
502 changes in AHR between WT and IgM$^{-/-}$ were associated with muscle system
503 processes and skeletal muscle contraction (Fig. 3f). There was also an over-
504 representation of gene ratios associated with skeletal muscle development,

505 differentiation and contraction, and suppression of genes associated with chemotaxis
506 and plasma membrane-bounded cell projection (Supplementary Fig. 7).
507
508 ***BAIAP2L1* is expressed in lung cells in contact with airway smooth muscle cells.**
509 We decided to focus on *Baiap2l1* also known as Inverse-bin-amphiphysin-Rvs (I-
510 BAR)-domain-containing protein insulin receptor tyrosine kinase substrate (IRTKS),
511 which has been shown to promote actin polymerisation and microvilli length in the
512 intestinal epithelial cells [40]. We first verified whether BAIAP2L1 was also
513 downregulated at the protein level in IgM-deficient mouse lungs challenged with HDM
514 (Fig. 4a). We found lower expression levels of BAIAP2L1 in IgM-deficient mice
515 compared to WT mice challenged with HDM by western blotting, although this was not
516 significant (Fig. 4a). Human Protein Atlas search suggested that BAIAP2L1 is
517 expressed by multiple cell types including fibroblasts, skeletal muscle, smooth muscle
518 and macrophages [41]. We then investigated by immunofluorescence which cell types
519 within the lung could be expressing BAIAP2L1 (Fig. 4b). We found BAIAP2L1 to be
520 closely expressed within structural cells in close contact to smooth muscle cells (less
521 than 10μm), a cell type known to be essential in bronchoconstriction. Airway smooth
522 muscle together with the extracellular matrix contributes to smooth muscle
523 hypertrophy which causes the narrowing of the airways. These cells by histology
524 appear to be separated due to fixation methods but are mashed together, especially
525 during the remodelling of the airways [42]. IgM deficiency did not impact this expression
526 in cells in close contact with smooth muscle (Fig. 4b). Because both western blot and
527 immunofluorescent were inconclusive, we also verified the expression of BAIAP2L1
528 via flow cytometry (gating in Supplementary Fig. 8a) and found it to be expressed
529 mainly by alpha-smooth muscle cells and increased in expression in HDM treated mice

530 compared to PBS control mice (Fig. 4c). Furthermore, we showed a reduction in
531 BAIAP2L1 expression amongst alpha-smooth muscle cells but not other cells (CD45
532 positive or alpha-smooth muscle negative cells, Supplementary Fig. 8b) in IgM-
533 deficient mice compared to WT mice treated with HDM, although this did not reach
534 significance (Fig. 4c). Overall, this data suggested that BAIAP2L1 is reduced at RNA
535 and protein level and likely influenced the reduction of AHR in IgM-deficient mice. This
536 was consistent with gene set enrichment in our RNA seq data where there was a
537 dominance of genes associated with muscle contraction which regulates AHR.
538

539 **CRISPR-Cas9 deletion of *BAIAP2L1* leads to reduced airway smooth muscle**
540 **contraction at a single cell.**

541 To understand how *Baiap2l1*, one of the genes downregulated in IgM-deficient mice,
542 could influence AHR, we resorted to an *in vitro* model that allowed us to measure
543 contraction using fluorescently labelled elastomeric contractible surface (FLECS)
544 technology [43] (Fig. 5a). We opted for airway smooth muscle as it has been shown to
545 contribute to the narrowing of the airway during an allergic attack and together with
546 neighbouring cells such as extracellular matrix and immune cells are critical in
547 hypertrophy [42]. We chose the human bronchial smooth muscle cell (BSMCs) line as
548 *BAIAP2L1* is expressed in structural cells including muscle and epithelial cells, and
549 actin together with myosin is essential in muscle contraction [41]. To this end, we used
550 CRISPR-Cas9 technology to knock down *BAIAP2L1* in BSMCs (Supplementary Fig.
551 9a-b). We also included ERDR1 as one of the genes that were also downregulated in
552 IgM-deficient mice. BSMCs (160 000/well) were stimulated with 10μM acetylcholine
553 (ACh), 10 ng/mL of human TNF-α and 100 ng/mL IL-13, followed by transfection with
554 ribonucleoprotein (RNP) complexes containing single guide RNA targeting *BAIAP2L1*

555 and Cas9 for 48h (Fig. 5b). Transfected cells were seeded onto elastomeric patterns,
556 stimulated with the same stimulants for 3h and fixed in 4% paraformaldehyde, followed
557 by staining with DAPI and Phalloidin before imaging on Stellarvision microscope and
558 quantification (Fig. 5a). We validated the deletion of *BAIAP2L1* by PCR and showed
559 reduced expression of *BAIAP2L1* in ACh and TNF-α stimulated cells transfected with
560 *BAIAP2L1* sgRNA when compared to scramble sgRNA (Supplementary Fig. 9c, line
561 3 and 4 compared to line 5 and 6). We also detected low expression of BAIAP2L1 in
562 unstimulated sgRNA scramble and sgRNA *BAIAP2L1* transfected cells
563 (Supplementary Fig. 9c, lines 1 and 2). Transfections with sgRNA did not impact cell
564 viability (Supplementary Fig. 9d). As expected, BSMCs displayed a higher level of
565 contraction in TNF-α or IL-13 stimulated cells compared to unstimulated cells (Fig. 5b-
566 d). In BSMCs transfected with sgRNA-*BAIAP2L1* and -*ERDR1*, we saw a significant
567 reduction in contraction levels in TNF-α stimulated cells when compared to scramble
568 sgRNA transfected and stimulated cells (Fig. 5b, c). We saw no differences in
569 contraction between scramble sgRNA and sgRNA-*BAIAP2L1* and -*ERDR1* stimulated
570 with IL-13 (Fig. 5d).
571
572 ***BAIAP2L1* deletion but not *ERDR1* is essential in acetylcholine-induced smooth**
573 **muscle contraction.**
574 Contraction of the ASM is central to AHR as it controls airway diameter and airflow
575 which can increase resistance [20]. Airway smooth muscle contractility is induced when
576 extracellular factors such as ACh bind through muscarinic 3 acetylcholine receptor
577 (m_3AChR), activating a signalling cascade leading to calcium accumulation and
578 contraction [44]. We transfected BSMCs with sgRNA-*BAIAP2L1*, -*ERDR1* or scrambled
579 and stimulated cells with 10 μM ACh (Fig. 6a). We saw a significant reduction in BSMC

580 contraction transfected with sgRNA-*BAIAP2L1* when compared to scramble sgRNA
581 transfected and ACh stimulated (Fig. 6b-c). We saw no significant differences in BSMC
582 contraction between sgRNA-*ERDR1* transfected and scramble sgRNA transfected
583 and ACh stimulated cells (Fig. 6b-c). Taken together, this data indicates that
584 *BAIAP2L1* a gene that was downregulated in IgM-deficient mice has a stimulant-
585 specific role in inducing airway contraction of bronchial smooth muscle cells during
586 asthma.
587
588 **DISCUSSION**
589 Here, we described an unexpected function of IgM in the regulation of
590 bronchoconstriction. We show by RNA sequencing that in the lung tissue of IgM-
591 deficient mice, there is a reduction in genes (*Baiap2l1* and *Erdr1*) associated with actin
592 cytoskeleton and re-arrangement, a key factor in smooth muscle contraction and AHR.
593 We used single-cell force cytometry and CRISPR-Cas9 technology to validate these
594 genes in the human BSM cell line and show as a proof of concept that deletion of
595 *BAIAP2L1* reduced muscle contraction in a stimulant-specific manner.
596
597 B cells play a complex role in allergic asthma, earlier studies using B cell-deficient
598 mice showed a redundant role of B cells in OVA-induced allergic airway inflammation
599 and airway hyperreactivity [27–29]. We and others have recently shown using a more
600 complex allergen HDM relevant to human asthma that antigen load is crucial in B cell
601 function [22–24]. We explored these possibilities in the context of IgM deficiency and
602 observed a profound reduction in AHR. This was in complete contrast to what has
603 been observed in B cell-deficient mice and in IgE or FcεRI-deficient mice [23,24,30]. We
604 also found a similar reduction in AHR at higher doses of HDM, albeit less pronounced.

605 Reduction in AHR was not only specific to HDM, but we also found reduced AHR in
606 IgM-deficient mice sensitised with OVA complexed to alum and challenged with OVA,
607 although less pronounced. AHR reduction in IgM-deficient mice was also seen in the
608 acute papain model which only activates innate responses including innate lymphoid
609 cells [45]. Interestingly, this reduction in AHR was not associated with reduced allergic
610 airway inflammation including eosinophilia, mucus production or Th2 cells in all
611 models tested, which was unexpected considering these features are key in AHR. B
612 cell-deficient mice show a reduction in eosinophilia and antigen-specific Th2 cells at
613 low doses of HDM, which leads to reduced AHR [24]. Similar findings are observed in
614 mice lacking IL-4Rα specifically in B cells when challenged with HDM [22].
615
616 IgM deficiency did not impact B cell development in primary and secondary lymphoid
617 tissues and accumulation of follicular and germinal centre B cells. Interestingly, there
618 was a lack of class switching to IgG1 and IgE isotypes despite increased expression
619 of IgD. The lack of class switching to IgG1 and IgE contrasts with earlier reports, which
620 suggested that IgD can largely replace IgM for class switching to other isotypes,
621 resulting in delayed neutralising IgG1 against vesicular stomatitis virus (VSV) [32,46]. To
622 get a better understanding of which IgM function was responsible for AHR, we showed
623 that the transfer of naïve wild-type mice serum to IgM-deficient mice could restore IgE
624 production and HDM-specific IgE and IgG1. This is consistent with what has been
625 observed in the context of influenza viral infections, where the transfer of purified or
626 serum IgM into B cell-deficient mice restored IgM-induced viral neutralisation [47]. We
627 believe that naïve sera transferred to IgM-deficient mice were able to bind to the
628 surface of B cells via IgM receptors (FcμR / Fcα/μR), which are still present on IgM-
629 deficient B cells, and this signalling is sufficient to facilitate Class Switch

630 Recombination (CSR). This was also confirmed by the ability of B cells to reach
631 germinal centres in IgM-deficient mice during HDM exposure. Our IgM$^{-/-}$ mouse lacks
632 both membrane-bound and secreted IgM, and transferred serum contains at least
633 secreted IgM which can bind to B cell surfaces. Of course, we can't rule out that
634 transferred sera from WT mice also contains some IgG1 which can facilitate class
635 switching to IgE when transferred to IgM-deficient mice. Despite the ability of wild-type
636 serum to restore IgE, it was not enough to restore AHR, which may be due to the
637 difficulties in restoring IgM to normal levels (200-800 µg). Our findings on the
638 redundant role of IgE were consistent with previous studies where IgE nor its high-
639 affinity receptor (FcεRI) were essential in AHR in an HDM or OVA model [30]. The lack
640 of functional role of serum-transferred IgE was consistent with earlier findings on *H.*
641 *polygyrus* transfer of immune serum where IgE was found not to be essential in
642 protection against *H. polygyrus* re-infection [36]. Our efforts to adoptively transfer wild-
643 type bone marrow or sorted B cells into IgM-deficient mice were also largely
644 unsuccessful partly due to poor engraftment of wild-type B cells into secondary
645 lymphoid tissues. Natural secreted IgM is mainly produced by B1 cells in the peritoneal
646 cavity, and it is likely that any transfer of B cells via bone marrow transfer would not
647 be sufficient to restore soluble levels of IgM[3,10].
648
649 B cell isotype IgD has been shown to promote Th2 cells and OVA-, papain- and NP-
650 specific humoral responses specifically IgG1 and IgE through basophil activation [31].
651 IgD has also been shown to inhibit IgE-mediated basophil activation through
652 downregulation of genes associated with cytoskeleton organisation such as signal
653 transducers phosphoinositide-3 kinase, RAS, and RHO [31]. Our RNA sequencing data
654 showed downregulation of *Baiap2l1* and *Erdr1* in IgM-deficient mice, genes which

655 have been shown to associate with actin cytoskeleton and re-arrangement, [40,41,48].
656 Contraction of the ASM is central to AHR as it controls airway diameter and airflow
657 which can increase resistance [49]. ASM activated by cytokines such as IL-13 or TNF-α
658 or bronchoconstrictor ACh induces cytosolic calcium accumulation [49,50]. Ca^{2+} release
659 results in a cascade of events that involves kinases and phosphorylation of key
660 molecules such as actin and myosin involved in smooth muscle contraction [44]. Gene
661 set enrichment analysis suggested that genes downregulated in IgM-deficient mice
662 were involved in processes such as muscle contraction, muscle twitching, skeletal
663 muscle movement. As a proof of concept we validated the involvement of *BAIAP2L1*
664 in bronchial smooth muscle contraction using a high throughput method that allows us
665 to measure contraction of 1000s of single cells [43]. When we deleted *BAIAP2L1* using
666 CRISPR-Cas9, we showed that deletion of *BAIAP2L1* in BSMCs reduced smooth
667 muscle contraction when stimulated with TNF-α and ACh, but not IL-13. Deletion of
668 ERDR1 had minor impact on muscle contraction across different stimulants
669 suggesting a stimulant and gene-specific role. IRTKS/BAIAP2L1 has been shown to
670 regulate microvilli elongation by forming a complex with actin-regulating protein EPS8
671 [40]. In this setting IRTKS elongate microvilli via distinct mechanisms that require
672 functional WH2 and SH3 domains, which binds EPS8, an F-actin capping and bundling
673 protein [40]. We have not fully dissected how *BAIAP2L1* could be regulated by IgM, but
674 it is clear that through its actions to regulate actin bundling, it is involved in muscle
675 contraction which requires actin and myosin head interaction (summarised in Fig. 7).
676
677 We speculate that IgM can directly activate smooth muscle cells by binding a number
678 of its surface receptors including FcμR, Fcα/μR and pIgR [51–53]. IgM binds to FcμR
679 strictly, but shares Fcα/μR and pIgR with IgA [5,51,53]. Both Fcα/μR and pIgR can be

680 expressed by non-structural cells at mucosal sites [53,54]. We would not rule out that the
681 mechanisms of muscle contraction might be through one of these IgM receptors,
682 especially the ones expressed on smooth muscle cells[53,54]. Certainly, our future
683 studies will be directed towards characterizing the mechanism by which IgM potentially
684 activates the smooth muscle.
685
686 We believe these findings report for the first time an independent function of IgM from
687 its natural class switching and non-specific binding to microbial components. We
688 believe that IgM function in regulating ASM may be indirect through other unknown
689 factors but does not involve microbiota as treatment of mice with a mixture of
690 antibiotics did not restore AHR. Early vaccination with bacterial species, such as group
691 *A streptococcus* containing GlcNAc or β-1,3-glucans can protect adult mice against *A.*
692 *fumigatus*-induced allergic asthma [55]. This is mainly through conserved germline-
693 encoded IgM antibodies, which have broad specificities to common allergens
694 containing GlcNAc moieties such as Dermatophytes [8,56]. Together these findings
695 demonstrate for the first time an important function of IgM in regulating airway
696 hyperresponsiveness independent of the presence of T helper 2 allergic inflammation.
697 These findings have implications for future treatment of allergic asthma through
698 bronchodilators.
699
700 **Competing interests**
701 The authors declare that they have no competing interests.
702
703
704

705 **Acknowledgements**

706 We thank the UCT Research Animal Facility for maintaining mice, and Munadia Ansari
707 for genotyping mice. We are grateful to Lizette Fick and Raygaana Jacobs for their
708 excellent histology services and for confocal microscopy core facilities. We are grateful
709 to Ronnie Dreyer for the excellent cell sorting and Flow Cytometry Core Facility. We
710 thank FlowJo for proving free service to Africa.

711

712 **Author contributions**

713 Conceived and supervised study: SH FB. Performed the experiments: SH AFS JK KJ
714 NM MS AN FM HN WM. Analysed the data: SH AFS KJ JO NM HN FM. Wrote the
715 paper: SH FB. All authors discussed the results and commented on the manuscript.

716

717 **Funding statement**

718 This work was supported by ICGEB, Cape Town Component, Medical Research
719 Council (MRC) South Africa as well as support by the South African National Research
720 Foundation (NRF) Research Chair initiative (SARChi) and Wellcome Trust CIDRI-
721 Africa (203135Z/16/Z) to FB. SH is supported by NRF Thuthuka Grant (117721), NRF
722 Competitive Support for Unrated Researcher (138072), MRC South Africa under Self-
723 initiated grant. NM was supported by the South African MRC PhD Fellowship. AN was
724 supported by NRF MSc Scholarship. This research was funded in whole, or in part, by
725 the Wellcome Trust [Grant number 203135Z/16/Z]. For the purpose of open access,
726 the author has applied a CC BY public copyright licence to any Author Accepted
727 Manuscript version arising from this submission.

728

729 **References**

730 1. Akula, S., Mohammadamin, S. & Hellman, L. Fc Receptors for Immunoglobulins and
731 Their Appearance during Vertebrate Evolution. *PLoS One* **9**, e96903 (2014).
732 2. Blandino, R. & Baumgarth, N. Secreted IgM: New tricks for an old molecule. *J Leukoc*
733 *Biol* **106**, 1021–1034 (2019).
734 3. Baumgarth, N. *et al.* B-1 and B-2 Cell–Derived Immunoglobulin M Antibodies Are
735 Nonredundant Components of the Protective Response to Influenza Virus Infection.
736 *Journal of Experimental Medicine* **192**, 271–280 (2000).
737 4. Ehrenstein, M. R. & Notley, C. A. The importance of natural IgM: scavenger, protector
738 and regulator. *Nat Rev Immunol* **10**, 778–786 (2010).
739 5. Michaud, E., Mastrandrea, C., Rochereau, N. & Paul, S. Human Secretory IgM: An
740 Elusive Player in Mucosal Immunity. *Trends Immunol* **41**, 141–156 (2020).
741 6. Quartier, P., Potter, P. K., Ehrenstein, M. R., Walport, M. J. & Botto, M. Predominant
742 role of IgM-dependent activation of the classical pathway in the clearance of dying
743 cells by murine bone marrow-derived macrophages in vitro. *Eur J Immunol* **35**, 252–
744 260 (2005).
745 7. Wesemann, D. R. *et al.* Microbial colonization influences early B-lineage development
746 in the gut lamina propria. *Nature* **501**, 112–115 (2013).
747 8. New, J. S. *et al.* Neonatal Exposure to Commensal-Bacteria-Derived Antigens Directs
748 Polysaccharide-Specific B-1 B Cell Repertoire Development. *Immunity* **53**, 172-186.e6
749 (2020).
750 9. Kawahara, T., Ohdan, H., Zhao, G., Yang, Y.-G. & Sykes, M. Peritoneal Cavity B Cells
751 Are Precursors of Splenic IgM Natural Antibody-Producing Cells. *The Journal of*
752 *Immunology* **171**, 5406 LP – 5414 (2003).
753 10. Nguyen, T. T. T., Graf, B. A., Randall, T. D. & Baumgarth, N. sIgM–FcμR Interactions
754 Regulate Early B Cell Activation and Plasma Cell Development after Influenza Virus
755 Infection. *The Journal of Immunology* **199**, 1635 LP – 1646 (2017).
756 11. Jones, K., Savulescu, A. F., Brombacher, F. & Hadebe, S. Immunoglobulin M in Health
757 and Diseases: How Far Have We Come and What Next? . *Frontiers in*
758 *Immunology* vol. 11 2858 Preprint at (2020).
759 12. Yilmaz, B. *et al.* Gut Microbiota Elicits a Protective Immune Response against Malaria
760 Transmission. *Cell* **159**, 1277–1289 (2014).
761 13. Krishnamurty, A. T. *et al.* Somatically Hypermutated Plasmodium-Specific IgM+
762 Memory B Cells Are Rapid, Plastic, Early Responders upon Malaria Rechallenge.
763 *Immunity* **45**, 402–414 (2016).
764 14. Rapaka, R. R. *et al.* Conserved natural IgM antibodies mediate innate and adaptive
765 immunity against the opportunistic fungus Pneumocystis murina. *Journal of*
766 *Experimental Medicine* **207**, 2907–2919 (2010).
767 15. Subramaniam, K. S. *et al.* The absence of serum IgM enhances the susceptibility of
768 mice to pulmonary challenge with Cryptococcus neoformans. *J Immunol* **184**, 5755–
769 5767 (2010).
770 16. Magri, G. *et al.* Human Secretory IgM Emerges from Plasma Cells Clonally Related to
771 Gut Memory B Cells and Targets Highly Diverse Commensals. *Immunity* **47**, 118-
772 134.e8 (2017).

773 17. Weber, G. F. *et al.* Pleural innate response activator B cells protect against
774 pneumonia via a GM-CSF-IgM axis. *Journal of Experimental Medicine* **211**, 1243–1256
775 (2014).
776 18. del Barrio, L. *et al.* Production of Anti-LPS IgM by B1a B Cells Depends on IL-1β and Is
777 Protective against Lung Infection with Francisella tularensis LVS. *PLoS Pathog* **11**,
778 e1004706 (2015).
779 19. Goldstein, M. F. *et al.* Selective IgM immunodeficiency: retrospective analysis of 36
780 adult patients with review of the literature. *Annals of Allergy, Asthma & Immunology*
781 **97**, 717–730 (2006).
782 20. Lambrecht, B. N. & Hammad, H. The immunology of asthma. *Nat Immunol* **16**, 45–56
783 (2014).
784 21. Mandler, R., Finkelman, F. D., Levine, A. D. & Snapper, C. M. IL-4 induction of IgE class
785 switching by lipopolysaccharide-activated murine B cells occurs predominantly
786 through sequential switching. *The Journal of Immunology* **150**, 407 LP – 418 (1993).
787 22. Hadebe, S. *et al.* Deletion of IL-4Ra signaling on B cells limits hyperresponsiveness
788 depending on antigen load. *Journal of Allergy and Clinical Immunology* **148**, 99-109.e5
789 (2021).
790 23. Habener, A. *et al.* Regulatory B cells control airway hyperreactivity and lung
791 remodeling in a murine asthma model. *Journal of Allergy and Clinical Immunology*
792 **147**, 2281-2294.e7 (2021).
793 24. Dullaers, M. *et al.* House dust mite–driven asthma and allergen-specific T cells
794 depend on B cells when the amount of inhaled allergen is limiting. *Journal of Allergy*
795 *and Clinical Immunology* **140**, 76-88.e7 (2017).
796 25. Ballesteros-Tato, A. *et al.* T Follicular Helper Cell Plasticity Shapes Pathogenic T Helper
797 2 Cell-Mediated Immunity to Inhaled House Dust Mite. *Immunity* **44**, 259–273 (2016).
798 26. Wypych, T. P., Marzi, R., Wu, G. F. & Lanzavecchia, A. Role of B cells in T H cell
799 responses in a mouse model of asthma. *Journal of Allergy and Clinical Immunology*
800 **141**, 1395–1410 (2020).
801 27. MacLean, J. A., Sauty, A., Luster, A. D., Drazen, J. M. & De Sanctis, G. T. Antigen-
802 induced airway hyperresponsiveness, pulmonary eosinophilia, and chemokine
803 expression in B cell-deficient mice. *Am J Respir Cell Mol Biol* **20**, 379–387 (1999).
804 28. Hamelmann, E. *et al.* Development of Eosinophilic Airway Inflammation and
805 Airway Hyperresponsiveness Requires Interleukin-5 but Not Immunoglobulin E or B
806 Lymphocytes. *Am J Respir Cell Mol Biol* **21**, 480–489 (1999).
807 29. Korsgren, M., ält, J. S. E., Korsgren, O., Sundler, F. & Persson, C. G. A. Allergic
808 Eosinophil-rich Inflammation Develops in Lungs and Airways of B Cell–deficient Mice.
809 *Journal of Experimental Medicine* **185**, 885–892 (1997).
810 30. McKnight, C. G., Jude, J. A., Zhu, Z., Panettieri, R. A. & Finkelman, F. D. House Dust
811 Mite–Induced Allergic Airway Disease Is Independent of IgE and FcεRIα. *Am J Respir*
812 *Cell Mol Biol* **57**, 674–682 (2017).
813 31. Shan, M. *et al.* Secreted IgD Amplifies Humoral T Helper 2 Cell Responses by Binding
814 Basophils via Galectin-9 and CD44. *Immunity* **49**, 709-724.e8 (2018).
815 32. Lutz, C. *et al.* IgD can largely substitute for loss of IgM function in B cells. *Nature* **393**,
816 797–801 (1998).
817 33. Kirstein, F., Nieuwenhuizen, N. E., Jayakumar, J., Horsnell, W. G. C. & Brombacher, F.
818 Role of IL-4 receptor α–positive CD4+ T cells in chronic airway hyperresponsiveness.
819 *Journal of Allergy and Clinical Immunology* (2015) doi:10.1016/j.jaci.2015.10.036.

820 34. Wu, T. *et al.* clusterProfiler 4.0: A universal enrichment tool for interpreting omics
821 data. *The Innovation* **2**, (2021).
822 35. Muramatsu, M. *et al.* Class Switch Recombination and Hypermutation Require
823 Activation-Induced Cytidine Deaminase (AID), a Potential RNA Editing Enzyme. *Cell*
824 **102**, 553–563 (2000).
825 36. Wojciechowski, W. *et al.* Cytokine-Producing Effector B Cells Regulate Type 2
826 Immunity to H. polygyrus. *Immunity* **30**, 421–433 (2009).
827 37. Smith, F. L. *et al.* B-1 plasma cells require non-cognate CD4 T cell help to generate a
828 unique repertoire of natural IgM. *Journal of Experimental Medicine* **220**, e20220195
829 (2023).
830 38. Trompette, A. *et al.* Gut microbiota metabolism of dietary fiber influences allergic
831 airway disease and hematopoiesis. *Nat Med* **20**, 159–166 (2014).
832 39. Norderhaug, I. N., Johansen, F.-E., Krajči, P. & Brandtzaeg, P. Domain deletions in the
833 human polymeric Ig receptor disclose differences between its dimeric IgA and
834 pentameric IgM interaction. *Eur J Immunol* **29**, 3401–3409 (1999).
835 40. Postema, M. M., Grega-Larson, N. E., Neininger, A. C. & Tyska, M. J. IRTKS (BAIAP2L1)
836 Elongates Epithelial Microvilli Using EPS8-Dependent and Independent Mechanisms.
837 *Current Biology* **28**, 2876-2888.e4 (2018).
838 41. Abo, H. *et al.* Erythroid differentiation regulator-1 induced by microbiota in early life
839 drives intestinal stem cell proliferation and regeneration. *Nat Commun* **11**, 1–12
840 (2020).
841 42. James, A. L. *et al.* Airway Smooth Muscle Hypertrophy and Hyperplasia in Asthma. *Am*
842 *J Respir Crit Care Med* **185**, 1058–1064 (2012).
843 43. Pushkarsky, I. *et al.* Elastomeric sensor surfaces for high-Throughput single-cell force
844 cytometry. *Nat Biomed Eng* **2**, 124–137 (2018).
845 44. Ouedraogo, N. & Roux, E. Pulmonary & Respiratory Medicine Physiology of Airway
846 Smooth Muscle Contraction : An Overview. *J Pulm Respir Med* **4**, 1–6 (2014).
847 45. Darby, M. *et al.* ILC3-derived acetylcholine promotes protease-driven allergic lung
848 pathology. *Journal of Allergy and Clinical Immunology* **147**, 1513-1516.e4 (2021).
849 46. Ochsenbein, A. F. *et al.* Control of Early Viral and Bacterial Distribution and Disease by
850 Natural Antibodies. *Science (1979)* **286**, 2156 LP – 2159 (1999).
851 47. Jayasekera, J. P., Moseman, E. A. & Carroll, M. C. Natural Antibody and Complement
852 Mediate Neutralization of Influenza Virus in the Absence of Prior Immunity. *J Virol* **81**,
853 3487 LP – 3494 (2007).
854 48. Houh, Y. K., Kim, K. E., Park, H. J. & Cho, D. Roles of erythroid differentiation regulator
855 1 (Erdr1) on inflammatory skin diseases. *Int J Mol Sci* **17**, 1–10 (2016).
856 49. Perkins, C. *et al.* Selective stimulation of IL-4 receptor on smooth muscle induces
857 airway hyperresponsiveness in mice. *J Exp Med* **208**, 853–867 (2011).
858 50. Moulton, B. C. & Fryer, A. D. Muscarinic receptor antagonists, from folklore to
859 pharmacology; finding drugs that actually work in asthma and COPD. *Br J Pharmacol*
860 **163**, 44–52 (2011).
861 51. Nguyen, T. T. T. *et al.* The IgM receptor FcμR limits tonic BCR signaling by regulating
862 expression of the IgM BCR. *Nat Immunol* **18**, 321–333 (2017).
863 52. Shibuya, A. *et al.* Fcα/μ receptor mediates endocytosis of IgM-coated microbes. *Nat*
864 *Immunol* **1**, 441–446 (2000).
865 53. Liu, J. *et al.* Role of the IgM Fc Receptor in Immunity and Tolerance. *Front Immunol*
866 **10**, (2019).

54. Kim, M.-S. *et al.* A draft map of the human proteome. *Nature* **509**, 575–581 (2014).
55. Kin, N. W., Stefanov, E. K., Dizon, B. L. P. & Kearney, J. F. Antibodies Generated against Conserved Antigens Expressed by Bacteria and Allergen-Bearing Fungi Suppress Airway Disease. *The Journal of Immunology* **189**, 2246 LP – 2256 (2012).
56. Kearney, J. F., Patel, P., Stefanov, E. K. & King, R. G. Natural Antibody Repertoires: Development and Functional Role in Inhibiting Allergic Airway Disease. *Annu Rev Immunol* **33**, 475–504 (2015).

876 **FIGURE LEGENDS**

877

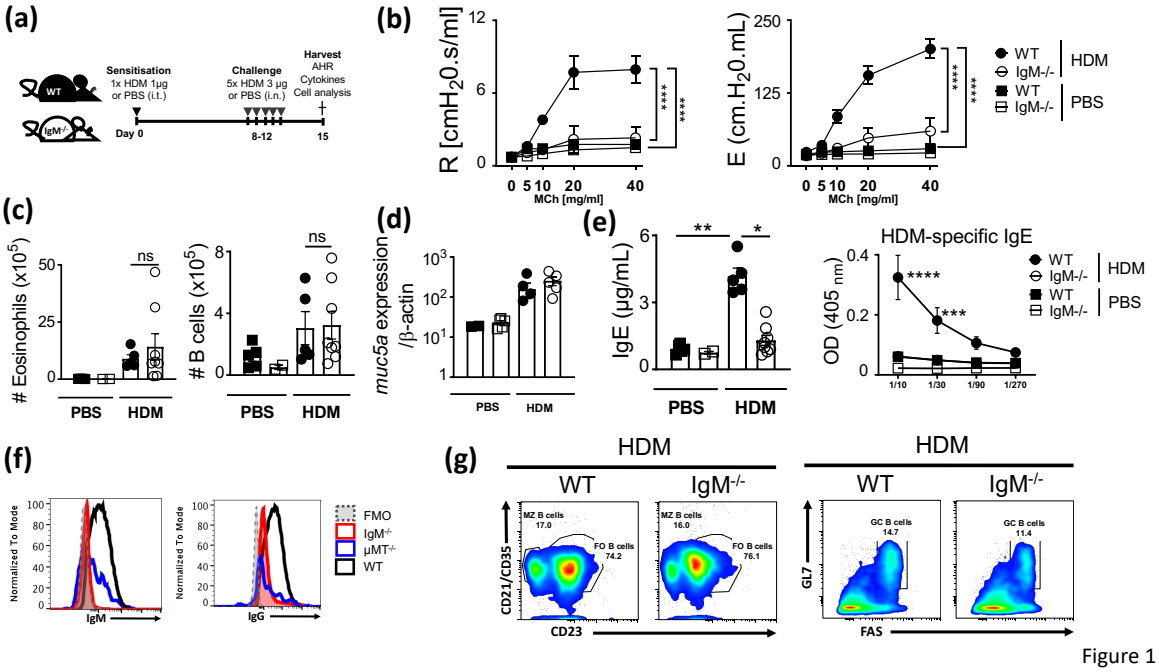

Figure 1

878

879 **Fig. 1 IgM-deficiency leads to reduced airway hyperresponsiveness and class**

880 **switching to IgE in HDM-induced asthma.**

881 **a** Schematic diagram showing sensitisation and challenge protocol where mice (IgM^{-}

882 $^{/-}$) and wild type littermate control (WT) were sensitised with HDM 1 µg intra-tracheally

883 on days 0 and challenged with HDM 3 µg on days 8-12. Analysis was done on day 15.

884 **b** Airway resistance and elastance were measured with increasing doses of acetyl

885 methacholine (0 -40 mg/mL).

886 **c** Total lung eosinophil numbers (live^{+}Siglec-F^{+}CD11c^{-}) and B cells

887 (live^{+}B220^{+}CD19^{+}MHCII^{+}) were stained and analysed by Flow cytometry and

888 enumerated from % of live cells.

889 **d** *Muc5a* gene expression in whole lung tissue.

890 **e** Total IgE and HDM-specific IgE in serum.

891 **f** IgG1 and IgM surface expression in mediastinal lymph node B cells of WT, $IgM^{-/-}$ and
892 $\mu MT^{-/-}$ mice.

893 **g** Marginal Zone ($live^{+}B220^{+}CD19^{+}MHCII^{+}CD21/CD35^{+}CD23^{-}$), follicular
894 ($live^{+}B220^{+}CD19^{+}MHCII^{+}CD23^{+}CD21/CD35^{+}$) and Germinal Centre
895 ($live^{+}B220^{+}CD19^{+}MHCII^{+}GL7^{+}FAS^{+}$) B cells in the mediastinal lymph node of WT and
896 $IgM^{-/-}$ mice challenged with HDM.

897 Shown is mean ± SEM from two pooled experiments (n=7 - 10). Significant differences
898 between groups were performed by Student *t*-test (Mann-Whitney) (c, d, e) or by Two-
899 Way ANOVA with Benforroni post-test (b) and are described as: *$p<0.05$, **$p<0.01$,
900 ***$p<0.001$, ****$p<0.0001$.

901

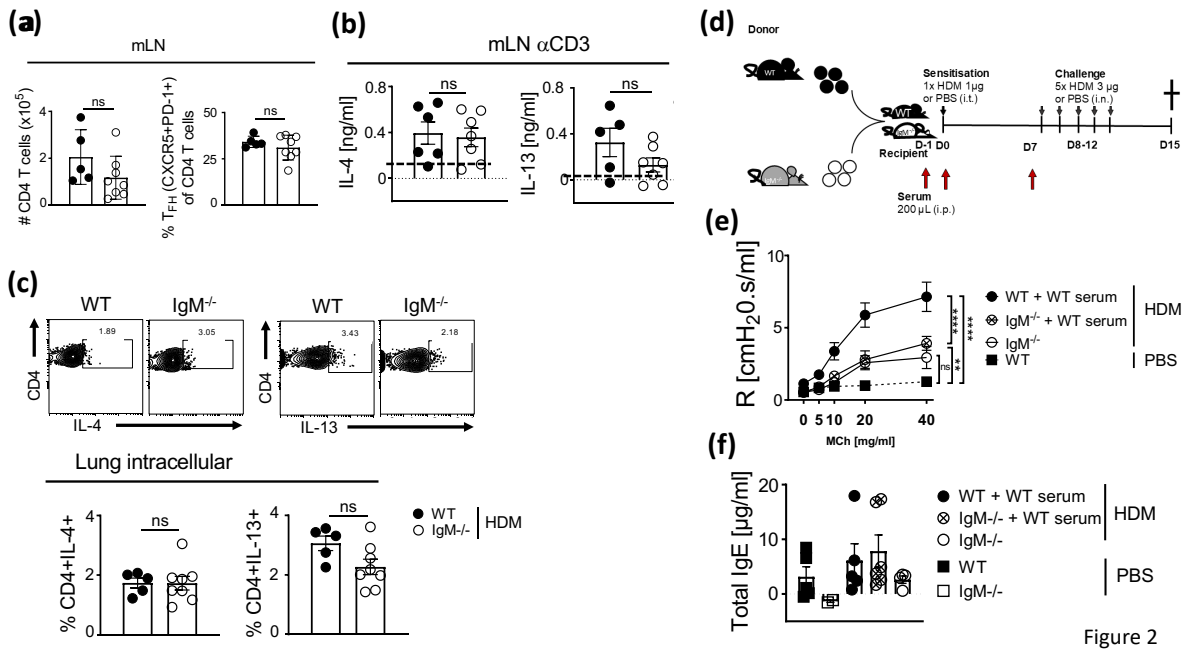

Fig. 2 IgM-deficiency does not lead to reduced Th2 allergic airway inflammation and serum transfer restores IgE, but not AHR. Fig. a-c, mice treated as in Fig. 1a.

a Total mediastinal lymph node CD4 T cell numbers (live$^+$CD3$^+$CD4$^+$) and % of Follicular Helper T cells (live$^+$CD3$^+$CD4$^+$PD-1$^+$CXCR5$^+$) of CD4 T cells were stained and analysed by Flow cytometry and enumerated from % of live cells.

b Mediastinal lymph nodes were stimulated with anti-CD3 (10µg/mL) for 5 days and supernatants were used to measure levels of IL-4 and IL-13. Cytokines were not detected in unstimulated or HDM (30µg) stimulated mLN.

c Representative FACS plots and frequencies of lung CD4 T cells (live$^+$CD3$^+$CD4$^+$) producing IL-4 and IL-13 after 5 hr stimulation with PMA/ionomycin in the presence of monensin.

d Schematic diagram showing serum transfer from WT to IgM$^{-/-}$ which were then sensitised as shown in Fig 1,a.

916 **e** Airway resistance was measured with increasing doses of acetyl methacholine (0 -
917 40 mg/mL).

918 **f** Total IgE in serum of mice either transferred with WT serum, $IgM^{-/-}$ serum or no
919 serum.

920 Shown is the mean ± SEM from two pooled experiments (n=5 - 8). Significant
921 differences between groups were performed by Student *t*-test (Mann-Whitney) (C, D,
922 E) or by Two-*Way ANOVA with Benforroni post-test (B) and are described as: *p<0.05,*
923 **p<0.01, ****p*<0.001, ******p*< 0.0001.

924

925

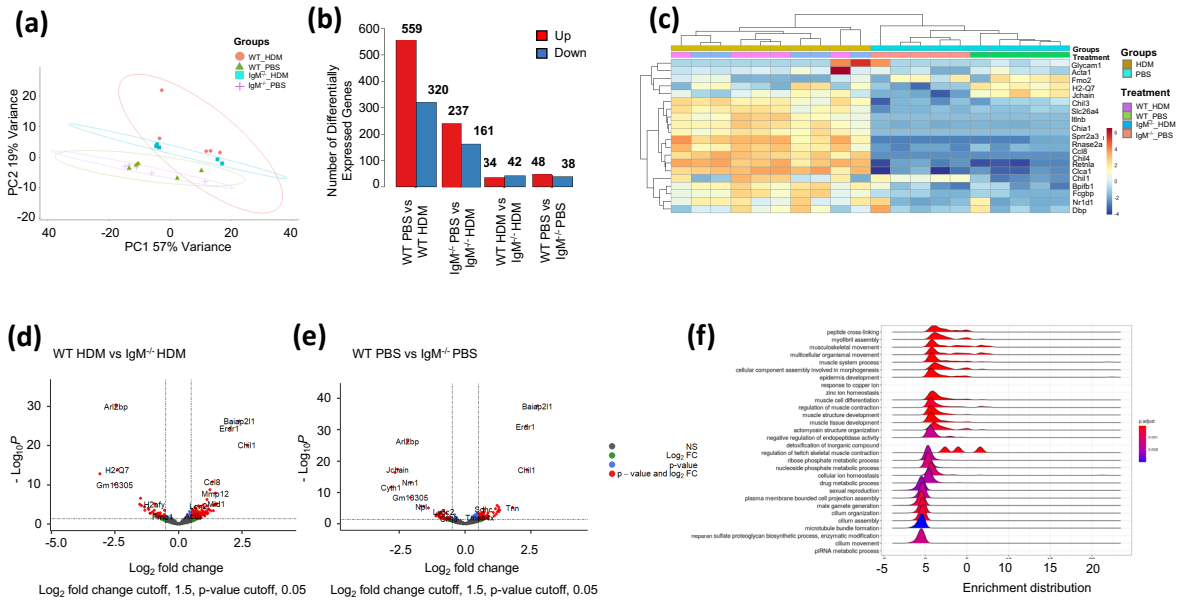

Figure 3

Fig. 3 Genes associated with muscle contraction are downregulated in IgM-deficient mice. WT and IgM$^{-/-}$ mice were treated as in Figure 1A and RNA was collected from the whole lung for RNA sequencing.

a Principal-component (PC) analysis showing variation in the global gene expression profiles across the different groups. PC1 (60%) and PC2 (18%), which capture the greatest variation in gene expression, are shown. Orange colour represents WT HDM, green colour represents WT PBS, Blue colour represents IgM$^{-/-}$ HDM and purple crosses represent IgM$^{-/-}$ PBS. Each dot represents an individual mouse.

b Number of differentially expressed genes between groups.

c Heatmaps depicting the differently expressed genes between WT and IgM$^{-/-}$ samples from HDM-treated and PBS mice ranked based on hierarchical clustering.

d-e Volcano plots: numbers and colour relate to genes that have an adjusted *p* value <0.05. Blue, significantly downregulated; red, significantly up regulated; grey, non-differentially expressed. P values were adjusted for multiple testing using the

942 Benjamini-Hochberg method. (D) represent changes between WT and IgM$^{-/-}$ treated
943 with HDM and (E) represents changes between WT and IgM$^{-/-}$ treated with saline.
944 **f** Gene set enrichment analysis (GSEA) of hallmark gene sets from the Molecular
945 Signatures Database of the Broad Institute, showing the normalized enrichment
946 scores (NES) for lung RNA-Seq data from WT mice.
947
948

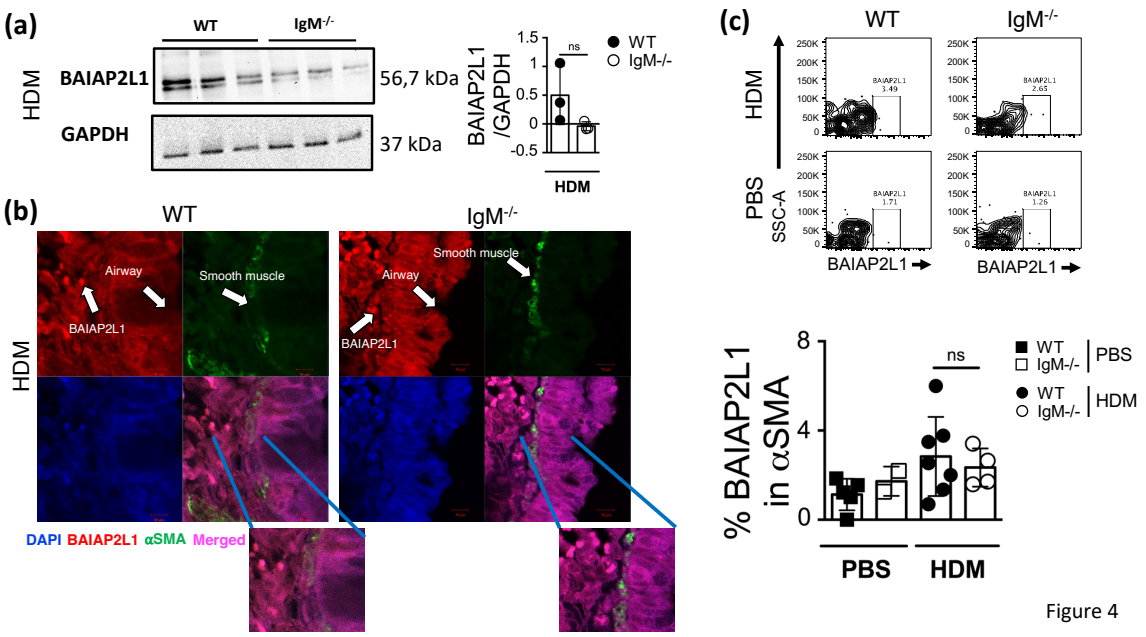

Figure 4

Fig. 4 *BAIAP2L1* is expressed in close contact to smooth muscle.

a Mouse lungs were homogenised in RIPA buffer and blotted on nitrocellulose. Rabbit anti-human BAIAP2L1 and mouse anti-GAPDH was used as primary antibody. Lines 1-3 is WT mice, lines 4-6 is IgM$^{-/-}$ mice sensitised and challenged with HDM.

b Lung sections from WT and IgM$^{-/-}$ mice sensitised and challenged with HDM were immunostained for nuclei stained DAPI (Blue), anti-BAIAP2L1 (red), α smooth muscle actin (green) and merged images (Magenta). Insert below shows zoomed in image of merged BAIAP2L1 and α smooth muscle actin.

c Representative flow cytometry plots showing BAIAP2L1 expression (Live^{+}Singlets^{+}CD45^{-}α SMA^{+}BAIAP2L1^{+}) in WT and IgM$^{-/-}$ treated with HDM or PBS. Quantification of % BAIAP2L1 in α smooth muscle actin is shown.

Shown are representative images from 2 independent experiments (n= 3 mice per group).

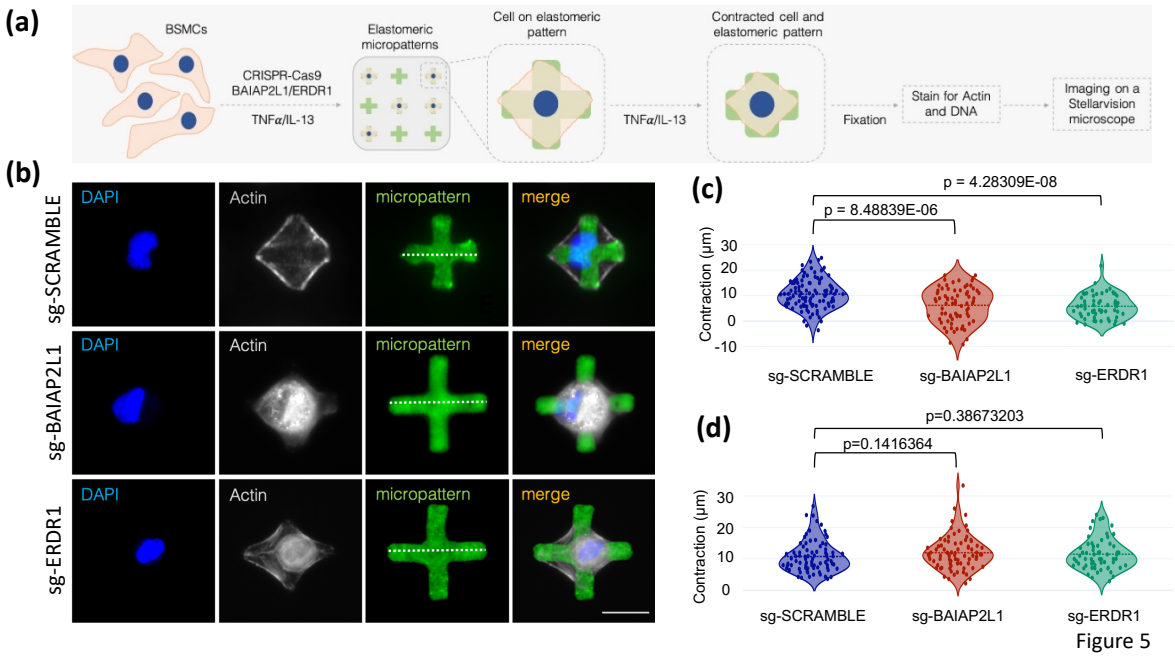

Fig. 5 CRISPR-based deletion of *BAIAP2L1* leads to reduced smooth muscle contraction at a single-cell level.

a, Bronchial smooth muscle cells ($1.6x10^5$ cells/well) were transfected with CRISPR-Cas9 single guide RNAs (scramble, *BAIAP2L1* and *ERDR1*), stimulated with recombinant human IL-13 (100 ng/mL) and TNF-α (10 ng/mL) for 48 h. Cells were then transferred to elastomeric micropatterns, stimulated again with rIL-13 and rTNF-α and fixed before imaging on a StellarVision microscope. **b**, Representative images of single BSMCs on micropatterns from scramble, *BAIAP2L1* and *ERDR1* stimulated with 10 ng/mL TNF-α. DNA was stained with DAPI, actin fibers with Phaloidin-565 and elastomeric micropatterns are coated in Fibronectin-488. Merged images are shown on the right. **c**, Violin plots showing contraction of 50-100 cells/condition stimulated with 10 ng/mL TNF-α, individual dots represent a single cell contraction, where blue is scramble sgRNA, red is *BAIAP2L1* sgRNA and green is *ERDR1* is sgRNA. **d**, Violin plots showing contraction of 50-100 cells/condition stimulated with 100 ng/mL

982 IL-13, individual dots represent a single cell contraction, where blue is scramble
983 sgRNA, red is *BAIAP2L1* sgRNA and green is *ERDR1* is sgRNA.
984
985 Shown is mean ±SEMs from two pooled experiment (n=50 - 100). Significant
986 differences between groups were performed by student t-test (Mann-Whitney) and *p*
987 value is shown.
988

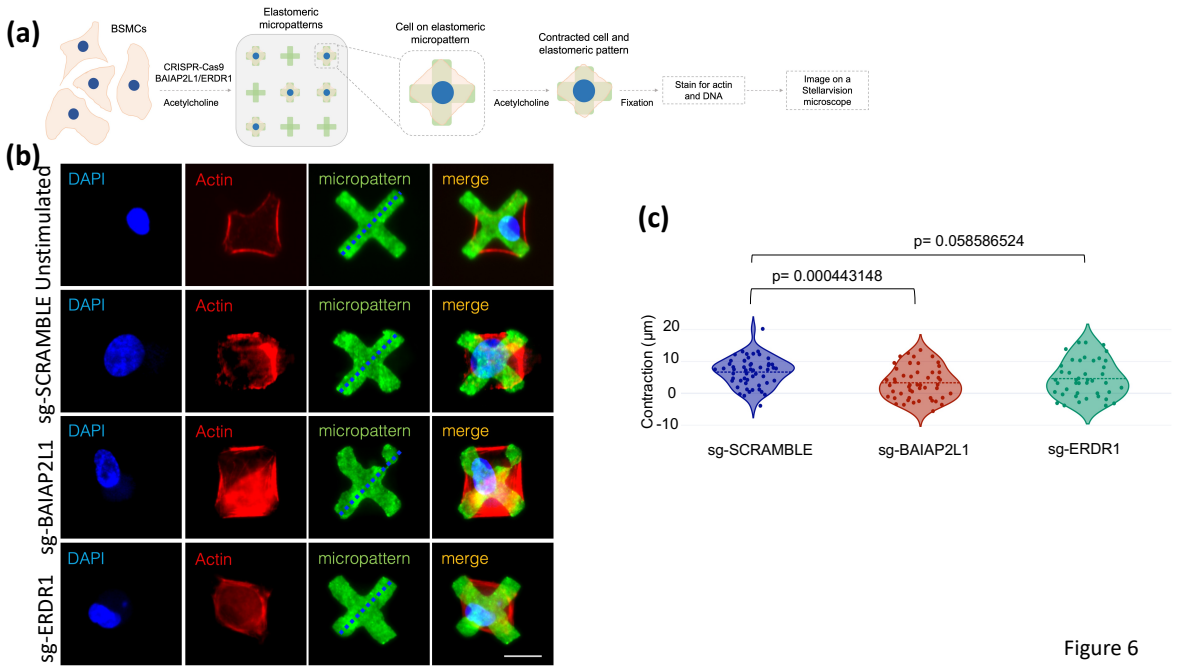

Figure 6

Fig. 6 CRISPR-based deletion of *BAIAP2L1* reduces smooth muscle contraction upon stimulation with acetylcholine.

a Bronchial smooth muscle cells ($1.6x10^5$ cells/well) were transfected with CRISPR-Cas9 single guide RNAs (scramble, *BAIAP2L1* and *ERDR1*), stimulated with Acetylcholine (10µM) for 48 h. Cells were then transferred to elastomeric micropatterns, stimulated again with ACh (10µM) and fixed before imaging on a StellarVision microscope.

b, Representative images of single BSMCs on a single micropattern from unstimulated, scramble, *BAIAP2L1* and *ERDR1* stimulated with ACh (10µM). Shown are DAPI, actin (red), a green fluorescent micropattern and merged images.

c, Violin plots showing contraction of 50-100 cells/condition stimulated with ACh (10µM) individual dots represent a single cell contraction, where blue is scramble sgRNA, red is BAIAP2L1 sgRNA and green is ERDR1 is sgRNA.

1004 Shown is mean ±SD from 1 representative experiment of 2 independent experiments

1005 (n=50 - 100). Significant differences between groups were performed by student t-test

1006 (Mann-Whitney) and *p* value is shown.

1007

1008

1009

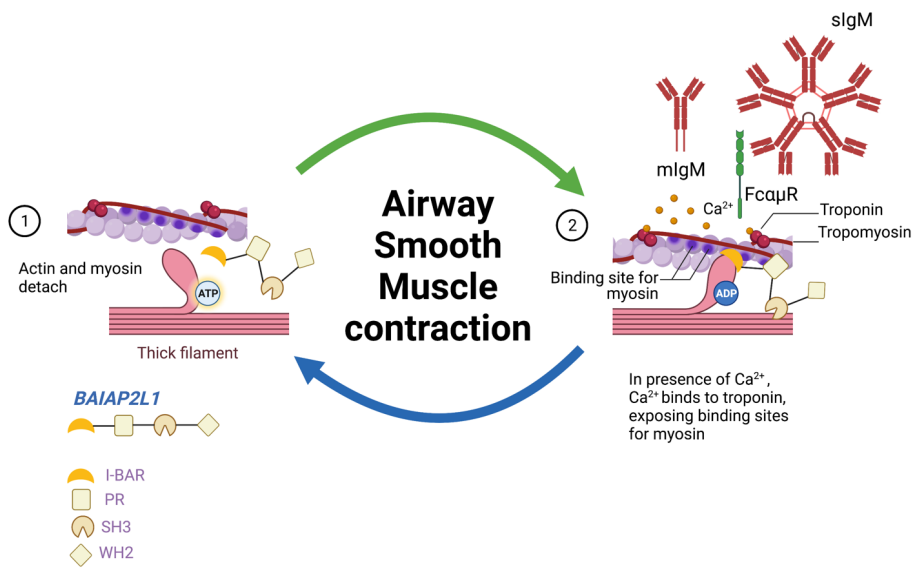

Figure 7

1010

1011 **Fig. 7 Working model showing how *Baiap2l1* could influence muscle contraction**

1012 **through influencing myosin and actin filament interaction. Image adapted from**

1013 **Biorender.**

1014